

5-2018

A Nanoindentation Study of the Fatigue Properties of Al/a-Si Core-Shell Nanostructures

Jason Steck

Follow this and additional works at: <http://scholarworks.uark.edu/meeguht>

 Part of the [Applied Mechanics Commons](#), [Nanoscience and Nanotechnology Commons](#), and the [Tribology Commons](#)

Recommended Citation

Steck, Jason, "A Nanoindentation Study of the Fatigue Properties of Al/a-Si Core-Shell Nanostructures" (2018). *Mechanical Engineering Undergraduate Honors Theses*. 68.
<http://scholarworks.uark.edu/meeguht/68>

This Thesis is brought to you for free and open access by the Mechanical Engineering at ScholarWorks@UARK. It has been accepted for inclusion in Mechanical Engineering Undergraduate Honors Theses by an authorized administrator of ScholarWorks@UARK. For more information, please contact scholar@uark.edu, ccmiddle@uark.edu.

A Nanoindentation Study of the Fatigue Properties of
Al/a-Si Core-Shell Nanostructures

A Nanoindentation Study of the Fatigue Properties of Al/a-Si Core-Shell Nanostructures

An Undergraduate Honors College Thesis

in the

Department of Mechanical Engineering
College of Engineering
University of Arkansas
Fayetteville, AR

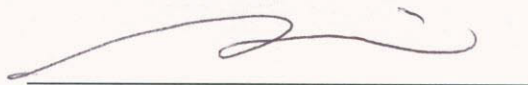
by

Jason G. Steck

April 17, 2017

This thesis is approved.

Thesis Advisor:



Min Zou

Thesis Committee:



Uchechukwu Wejinya



Min Zou

ABSTRACT

Nanostructure-textured surfaces can reduce friction and increase the reliability of micro- and nano-electromechanical systems (NEMS/MEMS). For MEMS incorporating moving parts, the fatigue properties of nanostructures pose a challenge to their reliability in long-term applications. In this study, the fatigue behavior of hemispherical Al/a-Si core-shell nanostructures (CSNs), bare hemispherical Al nanodots, and a flat Al/a-Si layered thin film have been studied using nanoindentation and nano-scale dynamic mechanical analysis (nano-DMA) techniques. Fatigue testing with nano-DMA shows that the deformation resistance of CSNs persists through 5.0×10^4 loading cycles at estimated contact pressures greater than 15 GPa. When the a-Si shell is removed, as in the Al nanodots, significant nanostructure deformation results due to repeated cyclic loading. In addition, for the Al/a-Si layered thin film, which lacks the geometry and core-confinement properties of CSNs, cyclic loading results in fatigue failure of the a-Si layer. CSNs demonstrate none of the failure mechanisms exhibited by these control structures. The unique properties displayed by CSNs when subjected to fatigue testing establish their prolonged durability when implemented in micro- and nano-scale applications.

KEY WORDS: core-shell nanostructure; nanoindentation; fatigue; dynamic mechanical analysis; continuous stiffness measurement

NOTE: This thesis, for the fulfillment of the requirements for the Mechanical Engineering Honors Program, is submitted in a journal format.

1. Introduction

Over the past decade, advancements in nanotechnology have allowed for the development of micro-/nano-electromechanical systems (MEMS/NEMS), which show great promise in nearly every product category. The applications of MEMSs range from aerospace to health care, and are commonly implemented as accelerometers [1], sensors [2], and magnetic storage devices [3]. However, when systems are designed at the micro- and nano-scale, the van der Waals force, capillary force, and electrostatic force are accentuated by the large surface-to-volume ratios compared to macroscale systems [4,5]. This results in a vulnerability to several failure mechanisms, including adhesion, stiction, and wear [4-7].

It is well understood that surfaces patterned with nanostructures, known as nanotextured surfaces (NTSs), significantly reduce adhesion and friction between the contact surfaces of many materials, and thus provide a solution to the current challenges of MEMS [8-14]. However, the individual nanotextures composing NTSs are susceptible to permanent deformation and fatigue failure under the contact stresses typically experienced in micro-scale devices [15-17]. For example, while microscale friction testing of Ni nanodot patterned surfaces showed a reduction in adhesion and friction, significant deformation was seen after testing [15,16]. This behavior has also been seen in Al nanotextured surfaces [14] and amorphous carbon surfaces [17]. Deformation and fracture in turn diminish the tribological properties initially provided by the textured surface.

Fatigue is of particular interest to the reliability of MEMS incorporating moving parts, since repetitive loading may lead to failure as a result of crack growth and the accumulation of plastic

deformation [6,7,18-22]. For example, single crystal silicon is the most predominantly used material in MEMS/NEMS due to its desirable electronic properties and mechanical resilience; however, research shows that at the micron-scale it has inferior wear and adhesion characteristics, as well as poor fatigue properties [22-25]. If NTSs are to be successfully implemented in micro-scale devices, the individual nanotextures must also not be susceptible to fatigue damage or wear.

Core-shell nanostructures (CSNs) composed of a soft Al core within a hard a-Si shell have been discovered to be highly deformation resistant, in addition to possessing superior tribological properties when implemented as deformation-resistant nanotextures [14,26]. Several studies have been performed to gain fundamental understanding of the mechanisms that contribute to their deformation resistance [27-29]. The sample surface consists of patterned hemi-spherical Al nanodots with 100 nm – 300 nm diameters on a silicon substrate. A 300 nm thick conformal a-Si shell is then deposited on the Al nanodot-patterned surface, forming core-shell nanostructures of a soft Al inner core encompassed by a hard a-Si shell. This nanotextured surface showed no permanent deformation when subjected to nanoscratch testing, with a maximum applied normal load of 8,000 μN with a 100 μm diamond tip. In addition, these structures have displayed superior resilience in nanoindentation testing, being subjected to high contact pressures with no residual deformation. However, their nanomechanical properties and deformation-resistance have not been studied beyond 4 loading/unloading cycles per structure and their structural integrity under prolonged repetitive loading has not been determined.

Nano-scale dynamic mechanical analysis (DMA) is a recently developed method of nanoindentation for characterizing visco-elasticity and fatigue life at the nano-scale [30,31]. By

superimposing a sinusoidal load-oscillation upon a nominally increasing indenter load, this technique allows for continuous measurement of the material properties of a sample. It has been shown previously that contact stiffness is sensitive to damage formation, and that continuous measurement of contact stiffness allows for precise characterization of a material's fatigue behavior [20]. This method has been used to determine the fatigue properties of Si nanobeams, Cu thin-films at the nano-scale, and amorphous carbon coatings [20,21,31]. In each study, an abrupt change in the contact stiffness indicated that fatigue damage had occurred.

In this paper, the method of nano-scale DMA is developed for studying the fatigue behavior of individual core-shell nanostructures. The fatigue properties of deformation-resistant Al/a-Si CSNs are then compared to the response of Al nanodots and flat Al/a-Si layered thin films subjected to repetitive loading. Scanning electron microscope images of the structures and surfaces are presented to better understand the mechanisms of failure, as well as to establish the deformation response of core-shell nanostructures under extended cyclic loading.

2. Experimental

2.1. Nanostructure Fabrication

Arrays of Al nanodots were fabricated using electron beam lithography (EBL) and a metal lift-off procedure. First, a positive tone electron resist, 495k MW PMMA at 4% dilution, was spin coated onto a (100) crystalline Si wafer at 3,000 rpm. An electron beam writer (JBX-9300FS, JEOL Ltd.) was used to selectively expose the electron resist, using a 50 kV accelerating voltage, 1 nA of current, and a beam

dose of $1,000 \mu\text{C}/\text{cm}^2$. The patterned arrays were then developed in a 1:3 mixture of methyl isobutyl ketone (MIBK) and isopropyl alcohol (IPA) for 45 s, and rinsed with pure IPA for 15 seconds. This resulted in patterned arrays of holes in the PMMA film, and was followed by a low-pressure oxygen plasma etch to smooth the edges of the holes. Next, 100 nm of Al was deposited onto the patterned PMMA film using thermal evaporation (Auto 306D, Edwards Vacuum) at a rate of 0.4 nm/s. Finally, the remaining PMMA was removed by immersion in a Remover PG (MicroChem Corp.) bath heated to 75°C for 48 hours. Using this fabrication method, ordered arrays of Al nanodots with base diameters of 100 nm and 300 nm were fabricated, each 100 nm in height.

The patterned arrays of 100 nm diameter Al nanodots were then coated with a-Si using plasma enhanced chemical vapor deposition (PECVD; Plasma-Therm SLR730). The rf power, substrate temperature, and silane flow rate during a-Si deposition were 20 W, 250°C , and 85 sccm, respectively. Using this method, a-Si was uniformly deposited on the sample, and Al/a-Si CSNs with 100 nm base diameter Al cores and an a-Si shell thickness of 300 nm were produced.

The flat Al/a-Si thin-films were fabricated using thermal evaporation followed by PECVD. First, 100 nm of Al deposited onto a (100) single crystal Si wafer using thermal evaporation (Auto 306D, Edwards Vacuum) at a rate of 0.4 nm/s. Then, 300 nm of a-Si was deposited onto the Al film by using PECVD with an rf power, substrate temperature, and silane flow rate of 20 W, 250°C , and 85 sccm, respectively. This resulted in flat Al/a-Si thin-films with an Al layer 100 nm thick and an a-Si layer 300 nm thick. Fig. 1 shows schematics of the three fabricated nanostructure geometries.

2.2. Fatigue and Nanoindentation Tests

Nanoindentation and fatigue experiments were carried out using a TriboIndenter (Hysitron Inc.) equipped with a NanoDMA I module. The Triboindenter operates by electrostatic force actuation and measures displacements using a capacitive sensing scheme, with a force resolution of 3 nN and a displacement resolution of 0.02 nm. Within the NanoDMA I module, a lock-in amplifier is used to apply a sinusoidal dynamic load to the indenter tip concurrently with a given quasi-static force, at frequencies between 0.1 Hz and 200 Hz. The lock-in amplifier continuously measures the displacement amplitude of the indenter tip and the phase shift between the indenter and the applied signal. From this data the dynamic material properties of the sample are determined. In this study, a spherical diamond indenter tip of 1 μm radius of curvature was used, and integrated scanning probe microscopy (SPM) within the TriboIndenter was used to accurately locate and indent the individual nanostructures with the same 1 μm tip. A large indenter tip radius, compared to the size of the nanostructures, was chosen to provide compression loading to the nanostructures, rather than penetration into the samples.

Fig. 2a shows a schematic of the tests performed on the Al nanodots and Al/a-Si thin film to determine the approximate load of failure due to dynamic loading. These tests were conducted in a load-controlled mode, incorporating a constant dynamic load amplitude and a mean quasi-static load increasing linearly throughout the experiment. To maintain uniform testing parameters across all geometries, Hertzian contact theory for sphere-on-sphere contact was used to estimate the contact pressure applied to the Al nanodots at the determined critical load [32]. The indentation force which applies an equivalent contact pressure to the CSNs was then calculated and used for fatigue testing of CSNs.

Fig. 2b shows a schematic of nanoindentation fatigue tests on hemi-spherical nanostructures and flat thin films. Fatigue testing was performed by maintaining a constant quasi-static load on the sample while applying a dynamic force at a given frequency. The maximum load amplitude was set to 70% of the determined critical load, and the excitation frequency was set to 60 Hz for all experiments. Contact stiffness change was used as an indicator of damage formation, and the number of cycles was determined by the time elapsed during each test [20]. To encourage deformation of the CSNs during fatigue loading, indents with larger quasi-static and dynamic load levels were also performed.

The nanoscale surface topography and morphology of the nanostructures were characterized with a combination of scanning electron microscopy (SEM; Nova NanoLab, FEI) and integrated SPM on the nanoindenter.

3. Results and Discussion

3.1. Nanostructure Characterization and Morphology

By using EBL to fabricate the patterned Al nanodots, very uniform arrays of Al nanodots and CSNs were produced. SEM micrographs of surfaces patterned with 300 nm diameter Al nanodots and CSNs with 100 nm core diameter and 300 nm shell thickness are shown in Fig. 3. Through X-ray diffraction measurements on a similarly prepared Al film, it was determined that the Al nanodots were polycrystalline, and composed of a mixture of (111) and (200) crystallites. Fig. 4 shows SEM images of an individual Al nanodot and CSN. The PECVD process followed for depositing a-Si resulted in small-scale surface roughness in the shell and film morphologies, but due to the large size of the indenter tip

used during nanoindentation, it is expected that this will not interfere with mechanical characterization of the structures.

3.2. Ramping Load Nanoindentation

3.2.1. Al Nanodots

Dynamic indentation experiments with a linearly increasing quasi-static load were performed to characterize the response of Al nanodots to dynamic compression loading, as well as to determine the load at which structural failure occurs. Fig. 5a shows a nanoindentation loading profile as a function of time from 50 μN to 300 μN increasing at 0.75 $\mu\text{N/s}$. This profile was used in conjunction with a 30 μN peak-to-peak dynamic load at an oscillation frequency of 60 Hz, such as shown in Fig. 2a, to indent a 300 nm diameter Al nanodot, while continuously measuring the contact stiffness of the nanostructure. Fig. 5b shows the contact stiffness and indenter displacement as functions of time for a 300 nm diameter Al nanodot indented with the previously defined loading profile. It is observed that a transition in contact stiffness occurs from linearly-increasing with time to scattered and increasing more gradually. In addition, it is seen that this transition coincides with a jump in displacement and a peak in contact stiffness, each occurring at a total applied load of approximately 120 μN . Fig. 5d and Fig. 5e show SPM topography and gradient images after indentation which indicate that cracking in the nanostructure has occurred. It is understood that the propagation of cracks within the nanostructure would manifest as discontinuities in the contact stiffness or displacement response, and it is strongly suggested that these correspond to the propagation of the observed cracks. Therefore, the critical load at which crack propagation occurs in a 300 nm Al nanodot due to dynamic loading was determined to be $\sim 120 \mu\text{N}$.

It should be noted that two additional smaller peaks in contact stiffness with corresponding displacement discontinuities were observed at mean applied loads of approximately 70 and 95 μN . The presence of two additional cracks in the nanostructure suggest that these signatures correspond to propagation of the second and third cracks. However, in order to investigate the most severe loading condition when applied to CSNs, 120 μN was chosen as the critical applied load due to dynamic loading.

3.2.2. Al/a-Si Layered Thin Film

Fig. 6a shows applied load versus displacement for a quasi-static indent peaking at 8000 μN on a flat Al/a-Si thin film with 100 nm of Al and 300 nm of a-Si deposited on Al. Here it is observed that two jumps in displacement occur at ~ 2000 and ~ 6000 μN , which are potential indications of mechanism activity within the structure. Fig. 6b shows contact stiffness versus mean applied load for a ramping load dynamic indentation test on the film. It is observed that as the applied load increases, a jump discontinuity in contact stiffness occurred at a maximum load of 1850 μN , with a magnitude of 1.8 N/mm. Looking at an SEM micrograph of the thin film surface after indentation at 8000 μN , shown in Fig. 7, it is clear that radial cracking, circumferential cracking, and delamination of the a-Si layer occur. Circumferential variations in contrast of the surface are potentially due to charging effects during SEM, which would result from a discontinuity between the two layers of the film. In addition, delamination of the a-Si film would occur prior to catastrophic failure, due to the distribution of tensile stress being maximized at the interface between the two materials. Therefore, it is suggested that the contact stiffness signature at 1850 μN seen in dynamic indentation corresponds to delamination of the a-Si layer. This is assumed to represent the same event which occurred at 2000 μN in quasi-static loading, since dynamic indentation applies a more severe loading condition and would result in a more rapid onset of failure. This conclusion is consistent with data from traditional nanoindentation of this structure at a variety of load levels, which show that

catastrophic failure of Al/a-Si thin films, including the propagation of cracks, occurs at approximately 6000 μN , as seen in Fig. 6a. Therefore, the mean critical load at which a flat Al/a-Si thin film fails due to quasi-static loading was determined to be $\sim 2000 \mu\text{N}$.

3.3. Fatigue Testing

3.3.1. Al Nanodot Fatigue Behavior

Nanoindentation fatigue testing was performed on 300 nm Al nanodots to characterize their behavior when subjected to cyclic loading. Fig. 8 shows contact stiffness as a function of cycles for a 300 nm diameter Al nanodot indented for 5.0×10^4 cycles at a mean load of 70 μN and a load oscillation amplitude of 30 μN . It was observed that the contact stiffness increased linearly during the first $\sim 1.0 \times 10^4$ cycles of loading, after which the stiffness plateaued and remained more or less constant for the remainder of the test. This initial trend of increasing contact stiffness may be attributed to both increasing contact area between the indenter tip and the nanostructure [33], as well as strain hardening due to dislocation nucleation and propagation in metals [34,35]. Fig. 9c and d show SPM images taken before and after fatigue testing, where it is seen that significant permanent deformation resulted in the nanostructure. Since the residual deformation is very large in comparison to the total height of the nanostructure, there is a large corresponding increase in contact area between the interfacing bodies. Therefore, increasing contact area is credited as the predominant source of the change in contact stiffness. Also, since all measurements are made after the first load cycle is applied, it is known that any delayed phenomena must be an effect of the applied load oscillation. Because of this, a trend of increasing contact stiffness strongly suggests that plastic deformation is occurring with each subsequent loading cycle, up until the contact stiffness plateaus at $\sim 1.0 \times 10^4$ cycles.

To further investigate this hypothesis, fatigue tests at the same load level were performed at up to 1.0×10^4 cycles, and contact stiffness versus cycles for this experiment is reported in Fig. 8. As before, the contact stiffness also transitioned from linear to constant. However, in contrast to the 5.0×10^4 cycle experiments, the time at which the structure remains at constant contact stiffness is greatly reduced because of the shorter testing time. Fig. 9a and b shows SPM micrographs of the Al nanodot after fatigue testing for 1.0×10^4 cycles, and Fig. 9c and d show SPM images of another Al nanodot tested for 5.0×10^4 cycles. Here it is observed that both nanostructures exhibit a permanent ~ 30 nm reduction in height. Thus, the cycles at which deformation ceases is defined as the point where contact stiffness remains constant, meaning that no further deformation is occurring past the first $\sim 1.0 \times 10^4$ cycle segment. It should be noted that although the Al nanodots exhibit prolonged fatigue life after 1.0×10^4 cycles, there remains significant permanent deformation in the nanostructure. This amount of residual deformation would render the structure ineffective for tribological and surface texturing applications, and should be classified as ductile failure of the nanostructure.

3.3.2. Fatigue Behavior of Flat Al/a-Si Thin Film

Fatigue testing was performed on flat Al/a-Si thin films to characterize the response of a layered material which lacks the geometric and core-confinement properties of standard CSNs. Fig. 10 shows contact stiffness versus cycles for fatigue tests on the Al/a-Si thin film at a 1300, 1400, 1500, and 1600 μN mean load and a unanimous 500 μN oscillating load amplitude. Due to the probabilistic nature of the failure signature appearing, fatigue tests at a variety of loads were conducted to establish the applied load which best captures fatigue failure, as well as to demonstrate the relationship between fatigue life and

applied mean stress. Fig. 10 shows contact stiffness for a 1300 μN mean applied load, where no change in stiffness is observed. This indicates that a 1300 μN mean load is not large enough to damage the film. At 1400 μN , a jump in contact stiffness of 1 N/mm was observed at 4.5×10^4 cycles. At subsequently higher applied mean loads, the number of cycles before which the failure signature appears decreases until 1600 μN , where the jump appears at only 0.4×10^4 cycles into testing. Following the argument presented for quasi-static nanoindentation experiments on this structure, a jump in contact stiffness at approximately 2000 μN corresponded to delamination between the a-Si and Al layers. Since the same failure signature presents itself in fatigue tests at slightly depressed load levels and with delayed occurrence, it is suggested that this discontinuity also corresponds to delamination or subsurface fracture of the film. Thus, the critical fatigue load is identified as $1400 \pm 250 \mu\text{N}$ (estimated contact pressure of ~ 19.4 GPa), below which no fatigue damage is induced within the structure for the duration tested.

3.3.3. Deformation Resistant CSNs

Nanoindentation fatigue testing was performed on CSNs to characterize their mechanical response to cyclic nanoindentation loading. From the experiments on 300 nm Al nanodots, the maximum contact pressure induced by an 85 μN applied load was estimated to be ~ 17.5 GPa. Hertzian Contact Theory was then used to transpose this pressure into the indenter force which applies an equivalent contact pressure to a CSN with a 100 nm core diameter and 300 nm thick shell, where it was assumed the CSN has an equivalent Young's modulus and Poisson's ratio based on the volumetric ratio of 20% Al and 80% a-Si. In this calculation, the values used for the Young's moduli are 170 GPa and 179 GPa for Al and a-Si, respectively, and the Poisson's ratios are 0.35 and 0.25 for Al and a-Si, respectively. This analysis yielded a mean indenter load of 55 μN and a peak-to-peak load amplitude of 30 μN .

Fig. 11a shows contact stiffness as a function of cycles for fatigue testing CSNs at a variety of load levels, including 55, 100, 150, and 200 μN mean loads superimposed with 30, 50, 75, and 100 μN oscillating load amplitudes, respectively. Three repetitions of each test show overlap in the stiffness response of individual nanostructures, which illustrates uniformity between nanostructures as well as repeatability of the testing procedure. Fig. 11b isolates one contact stiffness curve for each load level tested. The $55 \pm 15 \mu\text{N}$ indentation displays a contact stiffness response which increases gradually throughout the entirety of the test, resulting in a total stiffness increase of $\sim 1.5 \text{ N/mm}$ across 5.0×10^4 cycles. Unlike the fatigue response of bare Al nanodots, an increasing trend in contact stiffness of CSNs may correspond to mechanisms involving both core and shell materials. These include the accumulation of dislocations and strain hardening within the Al core, increasing contact area beneath the indenter tip, pressure induced phase transformations in a-Si [36], as well as a-Si densification occurring within the shell [25,37]. In Fig. 12a and b, SPM images of a CSN following $55 \pm 15 \mu\text{N}$ indentation show that no residual deformation is present in the nanostructure. In addition, nanoindentation testing on multiple structures resulted in a mean height change of 2 nm at $55 \pm 15 \mu\text{N}$. This eliminates increasing contact area as the primary source of this response, since progressive indenter displacement necessarily requires permanent deformation of the sample (i.e., if the elastic limit had not been surpassed by the initial loading cycle, there would be no further deformation due to subsequent cycles at the same load). In addition, nanoindentation experiments on a flat a-Si thin film show no evidence of a pressure-induced phase transformation up to an estimated contact pressure of $\sim 22 \text{ GPa}$ [29]. Since a-Si phase transformations and increasing contact area have been eliminated as potential sources of the increase in contact stiffness, it is suggested that a-Si densification and the accumulation of dislocations within the Al core are responsible.

This conclusion is consistent with experiments of repeated indentation on individual CSNs, which show hardening behavior with each subsequent indent [29].

Since no residual deformation was observed at the equivalent contact pressure of ~ 17.5 GPa, fatigue tests at incrementally higher applied loads were conducted to further investigate the resistance of CSNs to cyclic loading. It was observed that indents at 200 ± 50 μN showed a rapid increase in contact stiffness, followed by a well-defined plateau beginning at 1.0×10^4 cycles. Data from indents at intermediate load levels illustrate a relationship between increasing applied load and the rate of increasing contact stiffness, while the magnitude of total increase unanimously remained ~ 1.5 N/mm. Fig. 12c shows an SEM image of a CSN after indentation at 200 ± 50 μN for 5.0×10^4 cycles, where it is seen that even at the estimated contact pressure of ~ 25.1 GPa, there is no cracking or significant deformation present in the nanostructure. This is in contrast to the experiments conducted on the flat Al/a-Si layered structure, which exhibited visible cracking at an estimated ~ 19.4 GPa contact pressure.

To further investigate the response of CSNs subjected to high-pressure fatigue, fatigue testing was conducted at multiple test durations. Fig. 13 shows contact stiffness versus cycles for two separate CSNs undergoing fatigue testing at 200 μN mean load superimposed with 100 μN peak-to-peak oscillating load amplitude at 60 Hz frequency for 1.0×10^4 and 5.0×10^4 cycles. The two indentation curves closely overlap, displaying the same transition signature occurring at 1.0×10^4 cycles. Fig. 14 shows SPM images of CSNs fatigue tested at 200 μN mean load for 1, 1.0×10^4 , and 5.0×10^4 cycles, which display a residual change in height of 3, 11, and 9 nm, respectively. Through indentation of 3 structures for each test duration, the mean change in height was determined to be 4.3, 8.6, and 9.6 nm for each testing time,

respectively, with standard deviations of 1.3, 2.7, and 3.4 nm, respectively. These results are consistent with the observed contact stiffness trends, and show that deformation of the nanostructure, while minor, occurs mostly within the first 1.0×10^4 cycles of loading. In addition, the absence of further height reduction in the longest test duration entails that there is no permanent deformation occurring past the transition to constant contact stiffness, and suggests that the CSN exhibits superior fatigue life past this point.

It should be noted that although similar contact stiffness trends were witnessed in both Al nanodots and CSNs, the response provided by the CSNs is more consistent between independent nanostructures than the bare Al cores, in addition to lacking significant residual deformation. This suggests that a nanotexture composed of patterned CSNs would possess greater uniformity, and thus higher reliability and consistency in application. As a result, it is clear that even at high contact pressures, CSNs are very resistant to deformation when subjected to prolonged cyclic loading and CSNs do not exhibit the fatigue failure mechanisms present in either bare Al nanodots or flat Al/a-Si thin films.

4. Conclusions

The mechanical fatigue response of hemi-spherical Al nanodots, flat Al/a-Si layered thin films, and novel Al/a-Si core-shell nanostructures was characterized using nanoindentation and nano-scale DMA. The fatigue behavior of each nanostructure was analyzed through the change in contact stiffness throughout the applied loading cycles. The CSNs demonstrate superior deformation resistant properties when subjected to cyclic compression loading for 5.0×10^4 cycles, even at contact forces up to 250 μN (estimated contact pressure of 25.1 GPa). When the a-Si shell is removed, bare Al cores demonstrate

significant residual deformation due to repeated cyclic loading. The Al/a-Si thin films demonstrate delamination due to fatigue loading at contact pressures less than those applied to the CSNs. An analysis of the contact stiffness response of the CSNs show that dislocation nucleation and a-Si densification are occurring within the structure, resulting in hardening of the CSN with repeated loading. This study explicates that the novel deformation resistance of Al/a-Si CSNs persists through repeated loading cycles, and establishes their prolonged durability when implemented in nanomechanical applications.

5. Future Work

In this study, the experiments conducted to determine the fatigue behavior of a flat Al/a-Si layered thin film were not necessarily conclusive. An issue arose that although the nanoindentation results strongly suggest delamination between the a-Si and Al layers, this was not able to be captured through SEM imaging. When imaging was attempted, the fatigue testing location was not clearly defined, and it was not conclusive that failure of the surface occurred. This is likely due to one of two causes: recovery of the film surface over time, such that the indentation is not visually distinct, or displacement of the layers causing delamination, but the material recovers such that the a-Si and Al surfaces are separated but coincident.

To investigate the possibility of time-dependent recovery of the layered thin-film, SPM imaging before and after nanoindentation may be used. By imaging the indent location immediately afterwards, a measurable divot is present. Then, imaging the same location sometime later will allow direct analysis of whether the depth of the residual impression changes after indentation. This analysis will be sufficient in determining if time-dependent recovery of the nanostructure is occurring. In order to further investigate the mechanisms responsible for these failure signatures, focused ion beam (FIB) microscopy may be used

to cut a fatigue indentation impression along its cross-section. Then, SEM imaging may be used to directly analyze the interface between the Al and a-Si layers, where it will be clear whether delamination occurred.

ACKNOWLEDGEMENTS

The research was supported by the US National Science Foundation (NSF) under Grant Nos. CMS-1463306, and partial support from the Center for Advanced Surface Engineering under Grant No. OIA-1457888 and the Arkansas EPSCoR Program, ASSET III. We thank the Arkansas Biosciences Institute and the University of Arkansas for major equipment funding support, as well as the Arkansas Nano & Bio Materials Characterization Facility and the High Density Electronics Center for equipment use.

REFERENCES

- [1] Xu, R., Zhou, S., and Li, W. J., 2012, "MEMS Accelerometer Based Nonspecific-User Hand Gesture Recognition," *IEEE Sensors Journal*, **12**(5) pp. 1166-1173.
- [2] Liu, X., Mwangi, M., Li, X., 2011, "Paper-Based Piezoresistive MEMS Sensors," *Lab on a Chip*, **11**(13) pp. 2189-2196.
- [3] Eleftheriou, E., Antonakopoulos, T., Binnig, G. K., 2003, "Millipede - a MEMS-Based Scanning-Probe Data-Storage System," *IEEE Transactions on Magnetics*, **39**(2) pp. 938-945.
- [4] Komvopoulos, K., 2003, "Adhesion and Friction Forces in Microelectromechanical Systems: Mechanisms, Measurement, Surface Modification Techniques, and Adhesion Theory," *Journal of Adhesion Science and Technology*, **17**(4) pp. 477-517.
- [5] Kim, S. H., Asay, D. B., and Dugger, M. T., 2007, "Nanotribology and MEMS," *Nano Today*, **2**(5) pp. 22-29.
- [6] Walraven, J. A., 2003, "Failure mechanisms in MEMS," *Anonymous IEEE*, **1**, pp. 828-833.
- [7] van Spengen, W., 2003, "MEMS Reliability from a Failure Mechanisms Perspective," *Microelectronics Reliability*, **43**(7) pp. 1049-1060.
- [8] Jung, Y. C., and Bhushan, B., 2006, "Contact Angle, Adhesion and Friction Properties of Micro-and Nanopatterned Polymers for Superhydrophobicity," *Nanotechnology*, **17**(19) pp. 4970-4980.
- [9] Nair, R. P., and Zou, M., 2008, "Surface-Nano-Texturing by Aluminum-Induced Crystallization of Amorphous Silicon," *Surface & Coatings Technology*, **203**(5) pp. 675-679.
- [10] Zou, M., Cai, L., and Wang, H., 2006, "Adhesion and Friction Studies of a Nano-Textured Surface Produced by Spin Coating of Colloidal Silica Nanoparticle Solution," *Tribology Letters*, **21**pp. 25-30.
- [11] Zou, M., Seale, W., and Wang, H., 2005, "Comparison of Tribological Performances of Nanop and Micro-Textured Surfaces," *Proc. Inst. Mech. Eng. (J. Nanoeng. Nanosyst.)*, **219**pp. 103-110.

- [12] Zou, M., Cai, L., Wang, H., 2005, "Adhesion and Friction Studies of a Selectively Micro/Nano-Textured Surface Produced by UV Assisted Crystallization of Amorphous Silicon," *Tribology Letters*, **20**(1) pp. 43-52.
- [13] Song, Y., Nair, R., Zou, M., 2010, "Adhesion and Friction Properties of Micro/Nano-Engineered Superhydrophobic/Hydrophobic Surfaces," *Thin Solid Films*, **518**(14) pp. 3801-3807.
- [14] Morton, B., Wang, H., Fleming, R., 2011, "Nanoscale Surface Engineering with Deformation-Resistant Core-Shell Nanostructures," *Tribology Letters*, **42**(1) pp. 51-58.
- [15] Zou, M., Wang, H., Larson, P., 2006, "Ni Nanodot-Patterned Surfaces for Adhesion and Friction Reduction," *Tribology Letters*, **24**(2) pp. 137-142.
- [16] Wang, H., Nair, R., Zou, M., 2007, "Friction Study of a Ni Nanodot-Patterned Surface," *Tribology Letters*, **28**(2) pp. 183-189.
- [17] Lackner, J. M., Waldhauser, W., Major, L., 2013, "Tribology of Bio-Inspired Nanowrinkled Films on Ultrasoft Substrates," *Computational and Structural Biotechnology Journal*, **6**(7) pp. 2-12.
- [18] Saber-Samandari, S., and Gross, K. A., 2013, "Contact Nanofatigue shows Crack Growth in Amorphous Calcium Phosphate on Ti, Co-Cr and Stainless Steel," *Acta Biomaterialia*, **9**(3) pp. 5788-5794.
- [19] Pineau, A., Benzerga, A., and Pardoën, T., 2016, "Failure of Metals III: Fracture and Fatigue of Nanostructured Metallic Materials," *Acta Materialia*, **107**pp. 508-544.
- [20] Li, X., and Bhushan, B., 2003, "Fatigue Studies of Nanoscale Structures for MEMS/NEMS Applications using Nanoindentation Techniques," *Surface & Coatings Technology*, **163**pp. 521-526.
- [21] Liu, J., Xu, B., Wang, H., 2015, "Measurement for Mechanical Behavior and Fatigue Property of Cu Films by Nanoscale Dynamic Load Method," *Materials and Design*, **65**pp. 1136-1142.
- [22] Alsem, D., Pierron, O., Stach, E., 2007, "Mechanisms for Fatigue of Micron-Scale Silicon Structural Films," *Advanced Engineering Materials*, **9**(1-2) pp. 15-30.

- [23] Gaire, C., Ye, D., Lu, T., 2008, "Deformation of Amorphous Silicon Nanostructures Subjected to Monotonic and Cyclic Loading," *Journal of Materials Research*, **23**(2) pp. 328-335.
- [24] Ando, T., Shikida, M., and Sato, K., 2001, "Tensile-Mode Fatigue Testing of Silicon Films as Structural Materials for MEMS," *Sensors & Actuators: A.Physical*, **93**(1) pp. 70-75.
- [25] Kermouche, G., Barthel, E., Vandembroucq, D., 2008, "Mechanical Modelling of Indentation-Induced Densification in Amorphous Silica," *Acta Materialia*, **56**(13) pp. 3222-3228.
- [26] Tidwell, W., Scott, D., Wang, H., 2011, "Nanoindentation Study of Deformation-Resistant Al/a-Si Core-shell Nanostructures," *Acta Materialia*, **59**(15) pp. 6110-6116.
- [27] Fleming, R. A., and Zou, M., 2016, "Nanostructure-Textured Surfaces with Low Friction and High Deformation Resistance," *Tribology Transactions*, pp. 1-8.
- [28] Fleming, R. A., Goss, J. A., and Zou, M., 2017, "Material Dimensionality Effects on the Nanoindentation Behavior of Al/a-Si Core-Shell Nanostructures," *Applied Surface Science*, **412**pp. 96-104.
- [29] Fleming, R. A., and Zou, M., 2017, "The Effects of Confined Core Volume on the Mechanical Behavior of Al/a-Si Core-Shell Nanostructures," *Acta Materialia*, **128**pp. 149-159.
- [30] Li, X., and Bhushan, B., 2002, "A Review of Nanoindentation Continuous Stiffness Measurement Technique and its Applications," *Materials Characterization*, **48**(1) pp. 11-36.
- [31] Li, X., and Bhushan, B., 2002, "Development of a Nanoscale Fatigue Measurement Technique and its Application to Ultrathin Amorphous Carbon Coatings," *Scripta Materialia*, **47**(7) pp. 473-479.
- [32] Bhushan, B., 2013, "Introduction to Tribology," John Wiley & Sons, Ltd, pp. 91-155.
- [33] Pharr, G. M., Oliver, W. C., and Brotzen, F. R., 1992, "On the Generality of the Relationship among Contact Stiffness, Contact Area, and Elastic-Modulus during Indentation," *Journal of Materials Research*, **7**(3) pp. 613-617.

- [34] Li, J., Zhu, T., Van Vliet, K. J., 2002, "Atomistic Mechanisms Governing Elastic Limit and Incipient Plasticity in Crystals," *Nature*, **418**(6895) pp. 307-310.
- [35] Zhu, T., Li, J., Van Vliet, K., 2004, "Predictive Modeling of Nanoindentation-Induced Homogeneous Dislocation Nucleation in Copper," *Journal of the Mechanics and Physics of Solids*, **52**(3) pp. 691-724.
- [36] Domnich, V., Gogotsi, Y., and Dub, S., 2000, "Effect of Phase Transformations on the Shape of the Unloading Curve in the Nanoindentation of Silicon," *Applied Physics Letters*, **76**(16) pp. 2214-2216.
- [37] Perriot, A., Vandembroucq, D., Barthel, E., 2006, "Raman Microspectroscopic Characterization of Amorphous Silica Plastic Behavior," *Journal of the American Ceramic Society*, **89**(2) pp. 596-601.

LIST OF FIGURE CAPTIONS

Figure 1. Schematics of (a) Al/a-Si core-shell nano-structure, (b) Al nanodot, and (c) flat Al/a-Si layered material.

Figure 2. (a) Loading profile of a ramping-load indentation superimposed with a sinusoidal load oscillation. (b) Fatigue test loading profile of a sinusoidal load oscillation amplitude, P_{os} , superimposed upon a quasi-static load, P_{mean} , at a frequency, ω .

Figure 3. SEM micrographs of NTSs composed of (a) 300 nm diameter Al nanodots and (b) CSNs with 100 nm diameter cores and 300 nm shell thicknesses.

Figure 4. SEM micrographs of an individual (a) 300 nm diameter Al nanodot at a 45° oblique angle and (b) a top-view of a CSN with 100 nm core diameter and 300 nm a-Si shell thickness.

Figure 5. DMA indentation plots of (a) applied load vs. time and (b) contact stiffness vs. time for an Al nanodot undergoing ramping-load indentation of 50 to 300 μN quasi-static load superimposed with a 30 μN peak-to-peak dynamic load at an oscillation frequency of 60 Hz; SPM images of Al nanodot (c) before and (d) after nanoindentation, and (e) gradient image after nanoindentation (Arrows indicate points of failure).

Figure 6. (a) Load versus indenter depth for an Al/a-Si layered thin film indented with a maximum quasi-static load of 8000 μN . (b) Contact stiffness as a function of mean applied load for an Al/a-Si layered thin film indented with a quasi-static load increasing nominally from 1500-2000 μN , superimposed with an oscillation load amplitude of 200 μN at a frequency of 60 Hz.

Figure 7. SEM micrograph of the Al/a-Si thin film surface after quasi-static nanoindentation at a maximum applied load of 8000 μN .

Figure 8. Contact stiffness as a function of testing cycles for two individual Al Nanodots undergoing fatigue testing for 1.0×10^4 and 5.0×10^4 cycles at a constant $70 \mu\text{N}$ mean load superimposed with a $30 \mu\text{N}$ peak-to-peak load oscillation at a frequency of 60 Hz .

Figure 9. SPM images (a) before and (b) after dynamic indentation of a 300 nm Al nanodot for 1.0×10^4 cycles at a mean load of $70 \mu\text{N}$ superimposed with an oscillating load of $30 \mu\text{N}$ amplitude; SPM images (c) before and (d) after indentation of another Al nanodot for 5.0×10^4 cycles using the same loading profile.

Figure 10. Contact stiffness vs. cycles for an Al/a-Si layered thin film subjected to fatigue indentation at various mean loads superimposed with a $500 \mu\text{N}$ dynamic load at a 60 Hz frequency.

Figure 11. (a) Contact stiffness as a function of number of cycles for $55, 100, 150,$ and $200 \mu\text{N}$ quasi-static load indents on CSNs with a load amplitude of $30, 50, 75,$ and $100 \mu\text{N}$, respectively, with 3 repetitions at each indentation load. (b) Contact stiffness versus number of cycles for a single contact stiffness-time curve at each load level, with the magnitude of the initial and final data points labeled.

Figure 12. SPM images of a CSN (a) before and (b) after fatigue testing for 5.0×10^4 cycles at $55 \mu\text{N}$ mean load superimposed with $30 \mu\text{N}$ peak-to-peak oscillating load amplitude. (c) SEM image of CSN after fatigue testing for 5.0×10^4 cycles at $200 \mu\text{N}$ mean load superimposed with $100 \mu\text{N}$ peak-to-peak oscillating load amplitude.

Figure 13. Contact stiffness-cycles curve of $200 \mu\text{N}$ quasi-static load superimposed with a $100 \mu\text{N}$ peak-to-peak load oscillation on CSNs with 100 nm core and 300 nm shell for $10,000$ and $50,000$ cycles.

Figure 14. SPM images of CSNs with 100 nm core and 300 nm shell (a) before and (b) after nanoindentation for 1 cycle, (c) before and (d) after 1.0×10^4 cycles, and (e) before and (f) after

5.0×10^4 cycles at 200 μN quasi-static load superimposed with a 100 μN peak-to-peak oscillating load amplitude at 60 Hz frequency.

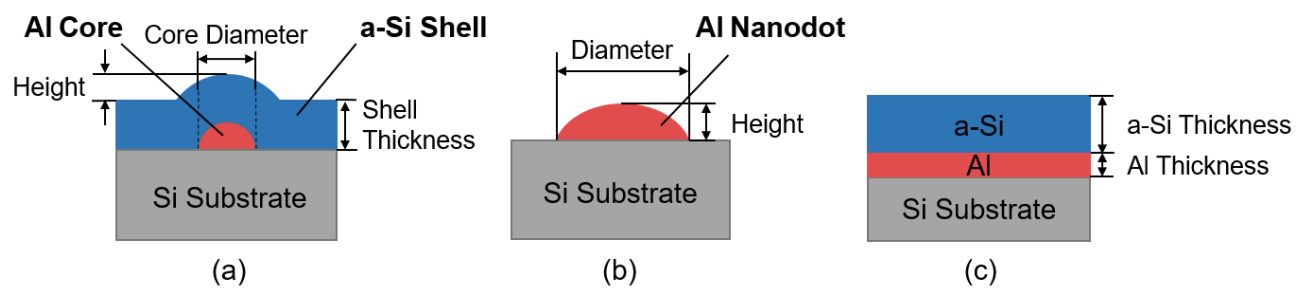


Figure 1: Schematics of (a) Al/a-Si core-shell nano-structure, (b) Al nanodot, and (c) flat Al/a-Si layered material.

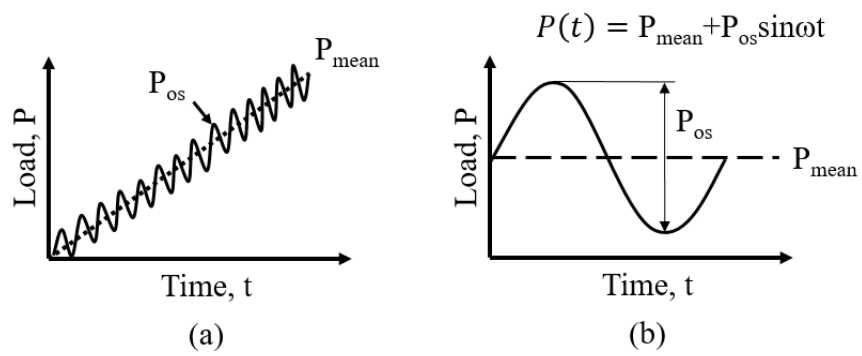


Figure 2: (a) Loading profile of a ramping-load indentation superimposed with a sinusoidal load oscillation. (b) Fatigue test loading profile of a sinusoidal load oscillation amplitude, P_{os} , superimposed upon a quasi-static load, P_{mean} , at a frequency, ω .

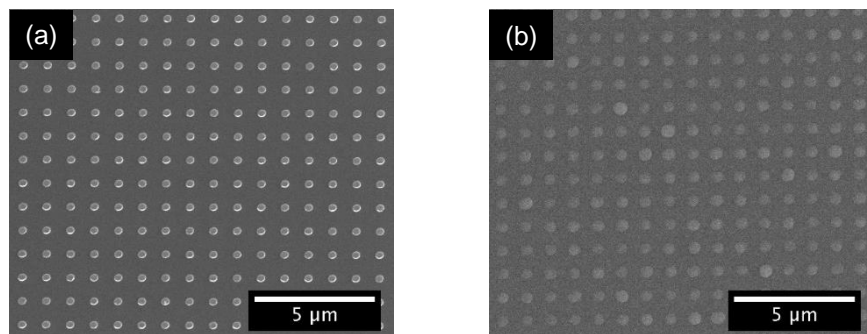


Figure 3: SEM micrographs of NTSs composed of (a) 300 nm diameter Al nanodots and (b) CSNs with 100 nm diameter cores and 300 nm shell thicknesses.

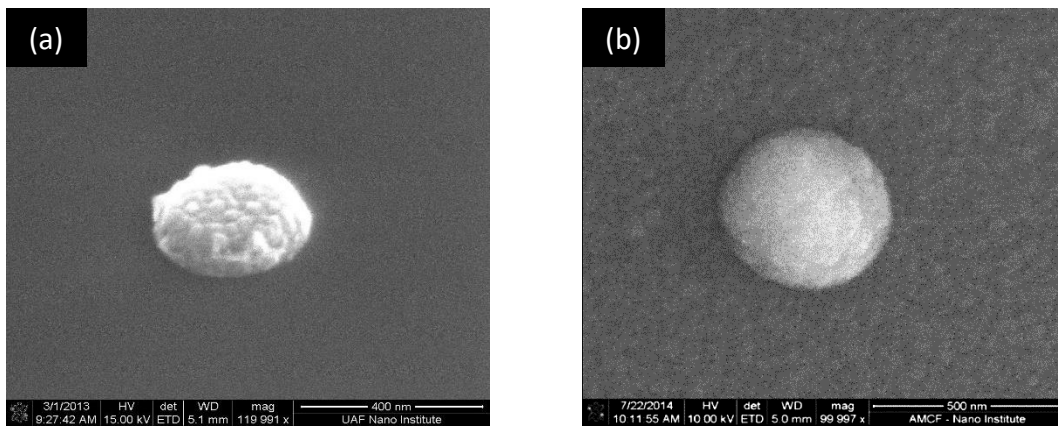
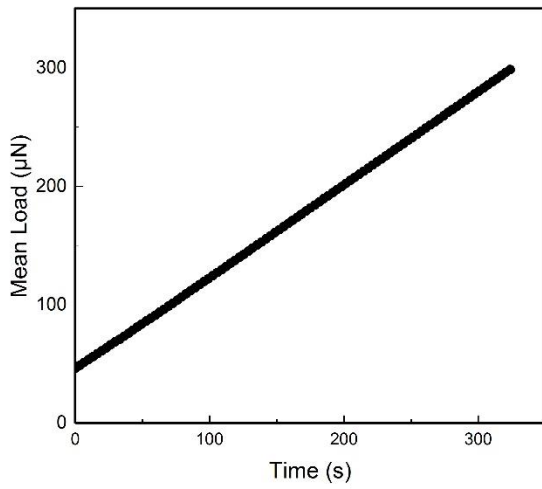
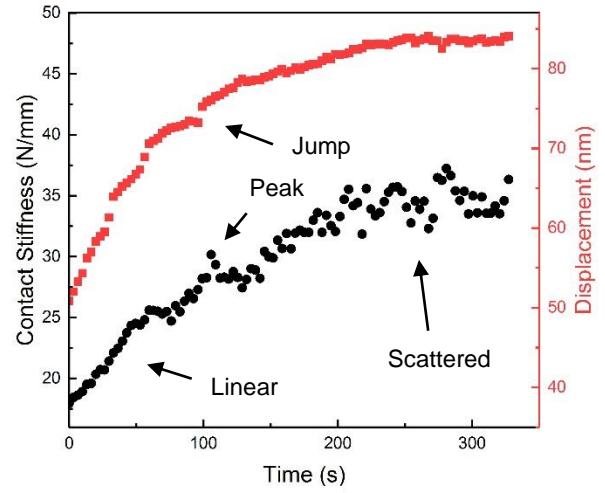


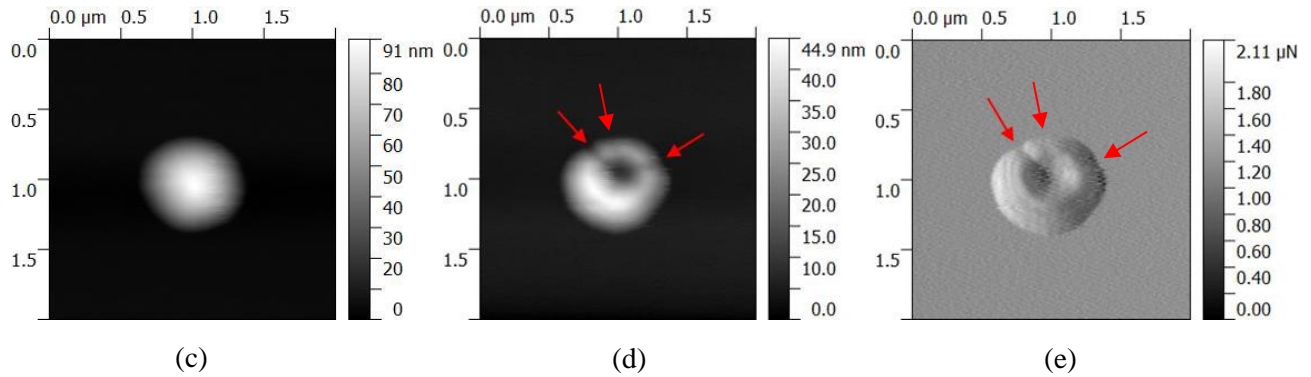
Figure 4: SEM micrographs of an individual (a) 300 nm diameter Al nanodot at a 45° oblique angle and (b) a top-view of a CSN with 100 nm core diameter and 300 nm a-Si shell thickness.



(a)



(b)



(c)

(d)

(e)

Figure 5: DMA indentation plots of (a) applied load vs. time and (b) contact stiffness vs. time for an Al nanodot undergoing ramping-load indentation of 50 to 300 μN quasi-static load superimposed with a 30 μN peak-to-peak dynamic load at an oscillation frequency of 60 Hz; SPM images of Al nanodot (c) before and (d) after nanoindentation, and (e) gradient image after nanoindentation (Arrows indicate points of failure).

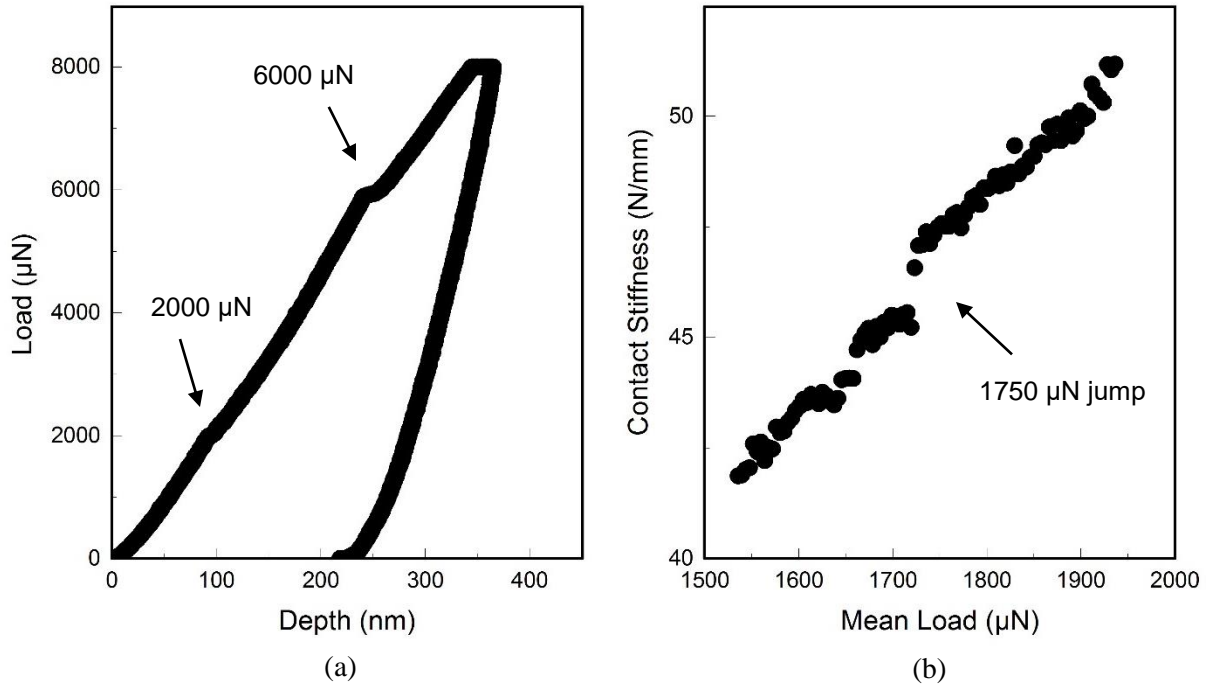


Figure 6: (a) Load versus indenter displacement for an Al/a-Si layered thin film indented with a maximum quasi-static load of 8000 μN . (b) Contact stiffness as a function of mean applied load for an Al/a-Si layered thin film indented with a quasi-static load increasing nominally from 1500-2000 μN , superimposed with an oscillation load amplitude of 200 μN at a frequency of 60 Hz.

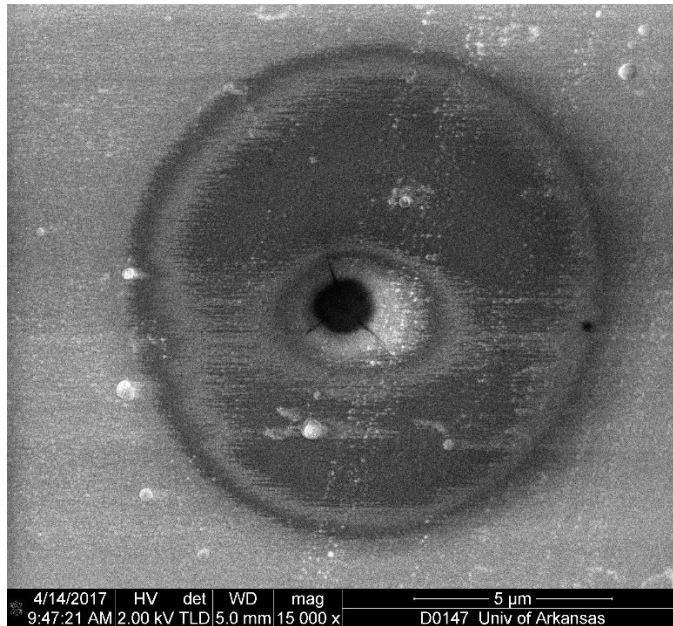


Figure 7: SEM micrograph of the Al/a-Si thin film surface after quasi-static nanoindentation at a maximum applied load of 8000 μN .

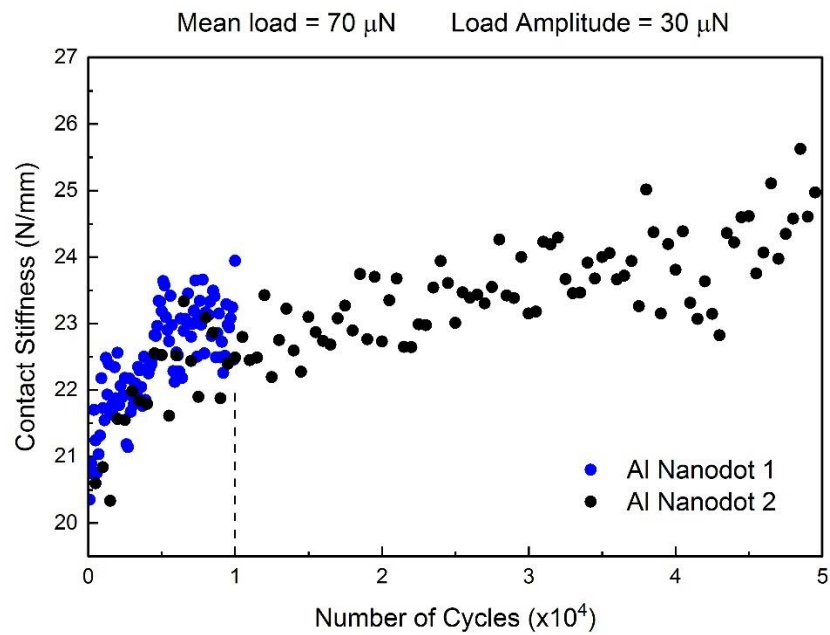


Figure 8: Contact stiffness as a function of testing cycles for two individual Al Nanodots undergoing fatigue testing for 1.0×10^4 and 5.0×10^4 cycles at a constant 70 μN mean load superimposed with a 30 μN peak-to-peak load oscillation at a frequency of 60 Hz.

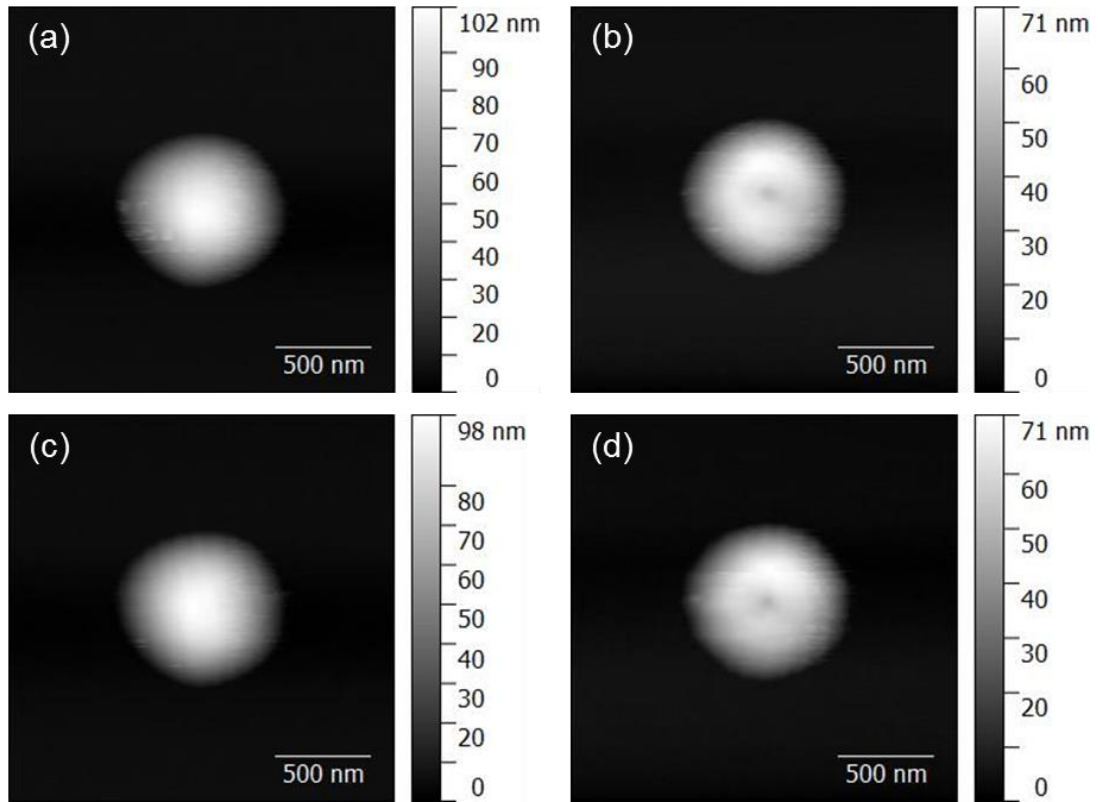


Figure 9: SPM images (a) before and (b) after dynamic indentation of a 300 nm Al nanodot for 1.0×10^4 cycles at a mean load of 70 μN superimposed with an oscillating load of 30 μN amplitude; SPM images (c) before and (d) after indentation of another Al nanodot for 5.0×10^4 cycles using the same loading profile.

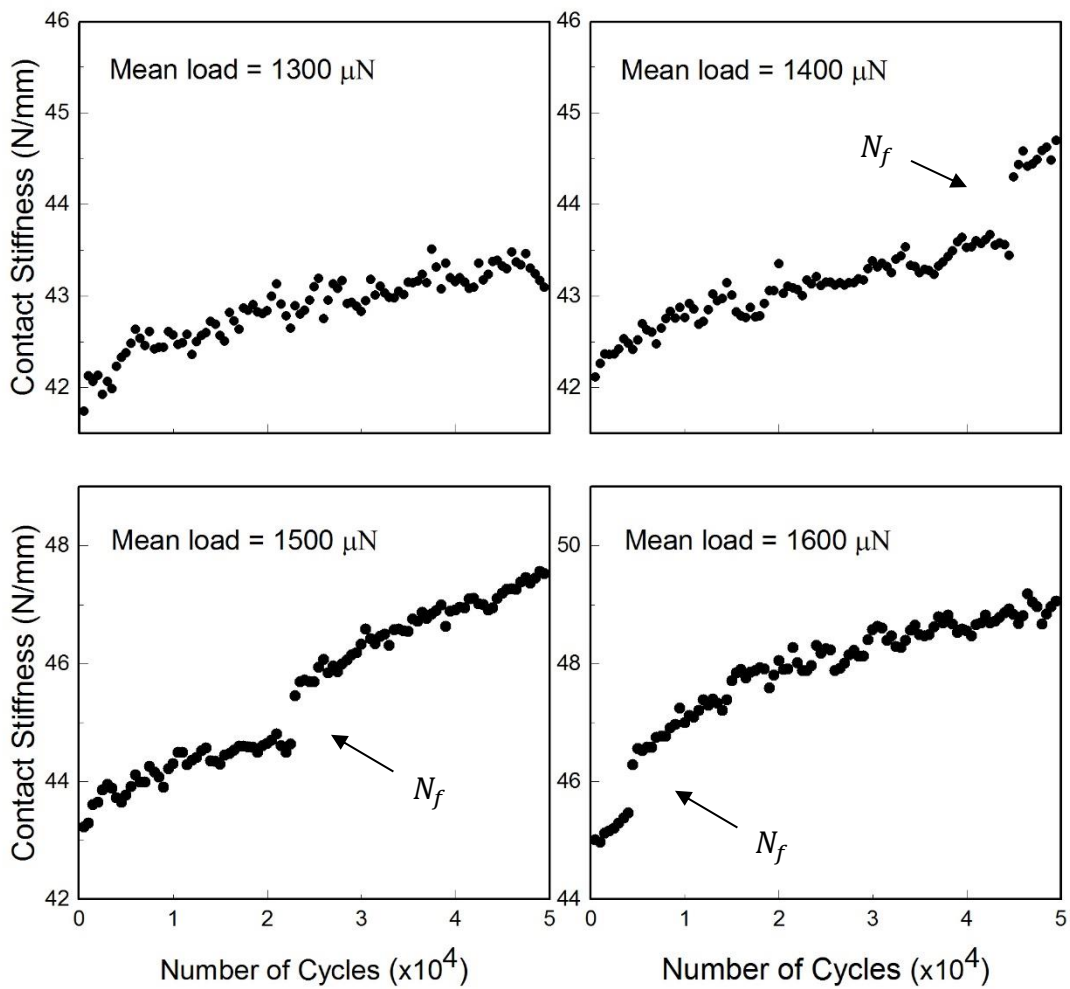
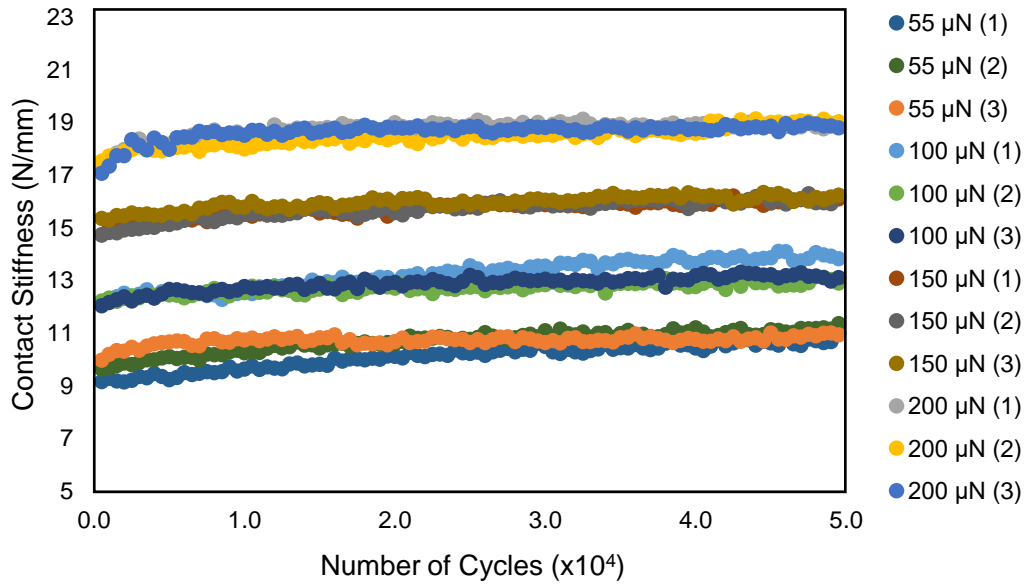
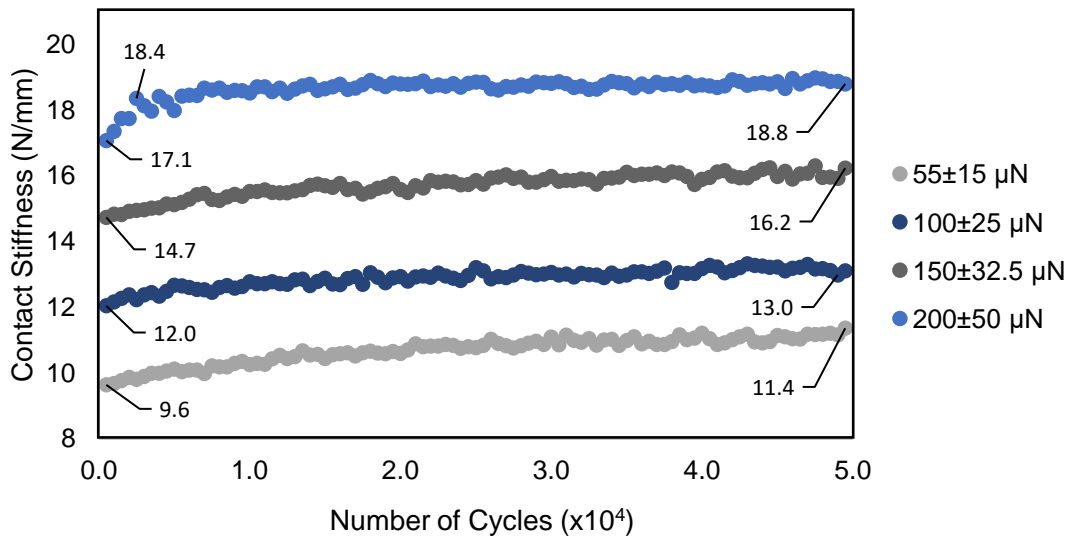


Figure 10: Contact stiffness vs. cycles for an Al/a-Si layered thin film subjected to fatigue indentation at various mean loads superimposed with a 500 μN dynamic load at a 60 Hz frequency.



(a)



(b)

Figure 11: (a) Contact stiffness as a function of number of cycles for 55, 100, 150, and 200 μN quasi-static load indents on CSNs with a load amplitude of 30, 50, 75, and 100 μN , respectively, with 3 repetitions at each indentation load. (b) Contact stiffness versus number of cycles for a single contact stiffness-time curve at each load level, with the magnitude of the initial and final data points labeled.

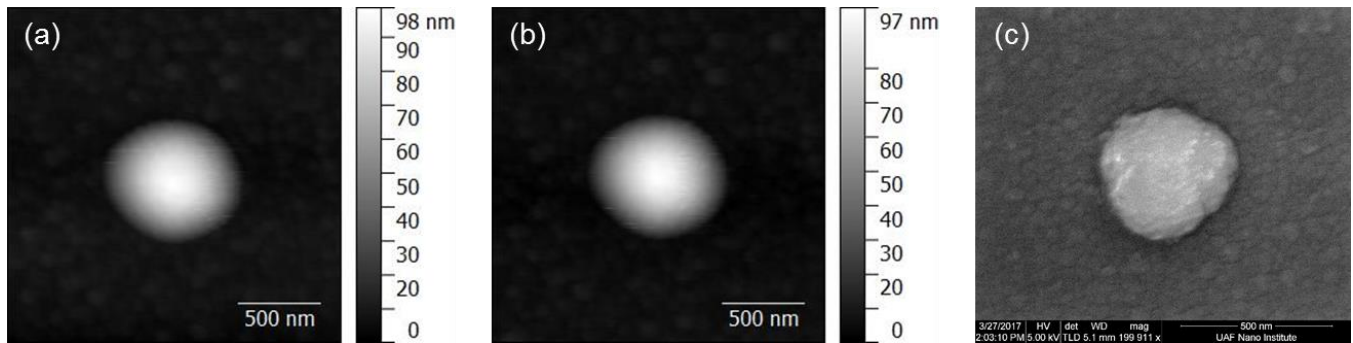


Figure 12: SPM images of a CSN (a) before and (b) after fatigue testing for 5.0×10^4 cycles at $55 \mu\text{N}$ mean load superimposed with $30 \mu\text{N}$ peak-to-peak oscillating load amplitude. (c) SEM image of CSN after fatigue testing for 5.0×10^4 cycles at $200 \mu\text{N}$ mean load superimposed with $100 \mu\text{N}$ peak-to-peak oscillating load amplitude.

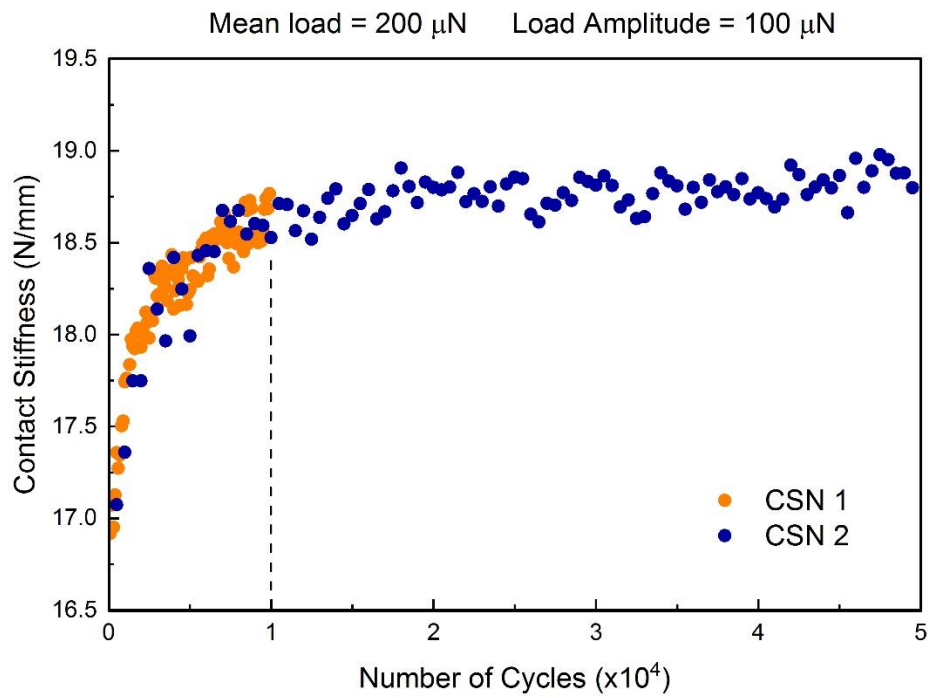


Figure 13: Contact stiffness-cycles curve of 200 μN quasi-static load superimposed with a 100 μN peak-to-peak load oscillation on CSNs with 100 nm core and 300 nm shell for 10,000 and 50,000 cycles.

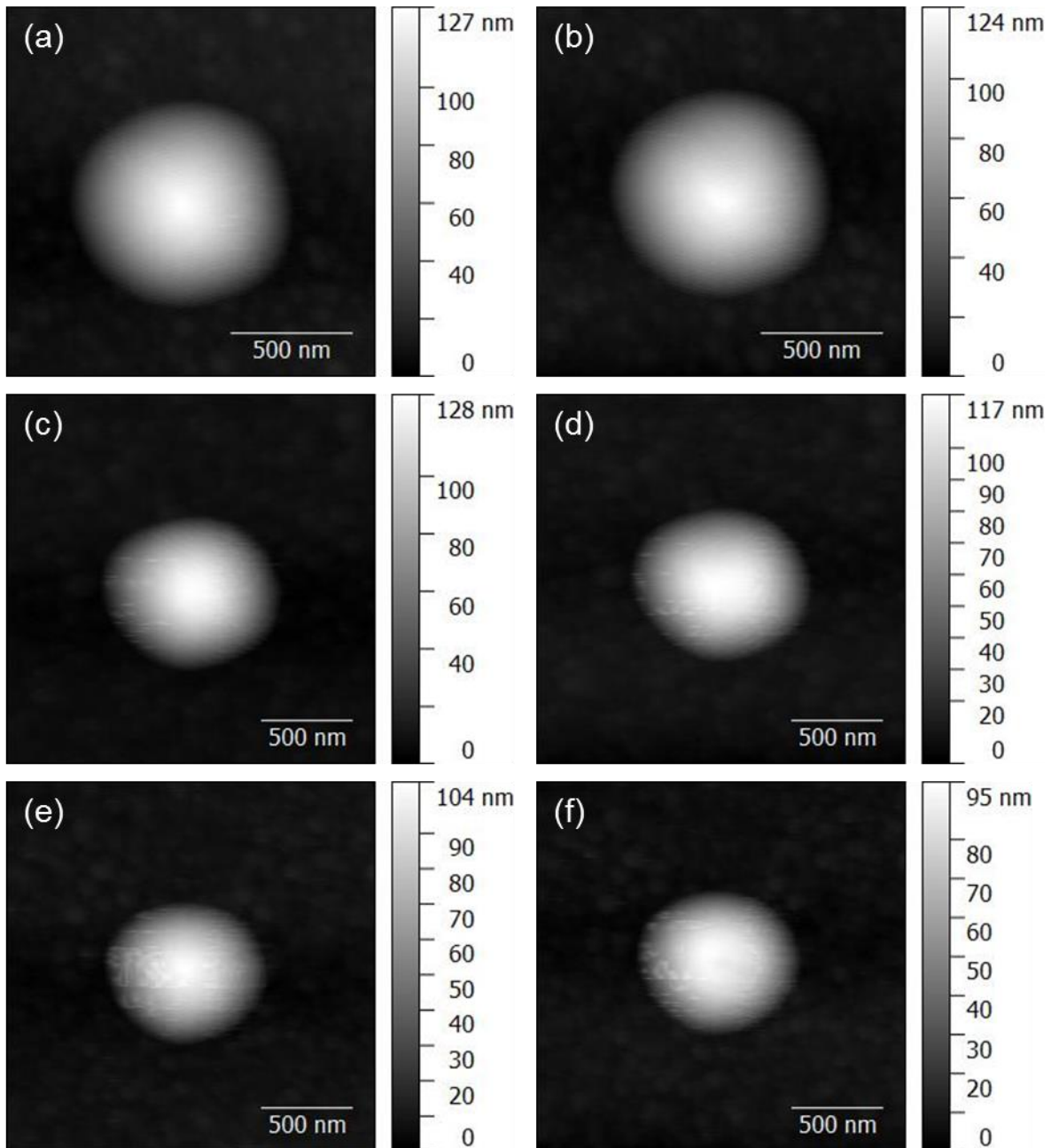


Figure 14: SPM images of CSNs with 100 nm core and 300 nm shell (a) before and (b) after nanoindentation for 1 cycle, (c) before and (d) after 1.0×10^4 cycles, and (e) before and (f) after 5.0×10^4 cycles at 200 μN quasi-static load superimposed with a 100 μN peak-to-peak oscillating load amplitude at 60 Hz frequency.